

Fundamental Studies on the Effect of Distortion Control Plans on Angular Distortion in Fillet Welded T-Joints

The effect of distortion control plans on the relationship between cumulative plastic strains and angular distortion in fillet welded T-joints was investigated

BY G. H. JUNG AND C. L. TSAI

ABSTRACT. The effect of external restraints and thermal management techniques (heat sinking and gas tungsten arc [GTA] preheating) on the relationship between cumulative plastic strains and angular distortion in fillet welded T-joints was investigated using plasticity-based distortion analysis (PDA). External restraints reduced the bend-up angular distortion by increasing the bend-down angular distortion induced by the transverse cumulative plastic strain. The higher restraint produces the less angular distortion. Heat sinking increases the bend-up angular distortion. This technique mainly controls the nominal cumulative plastic strains. The bend-down angular distortions induced by the transverse and vertical components are decreased. Those changes resulted in an increase of the total bend-up angular distortion.

Gas tungsten arc preheating reduced the angular distortion by decreasing the bend-up angular distortion induced by the xy-plane shear cumulative plastic strain. The characteristic relationship between cumulative plastic strains and angular distortion in fillet welded T-joints was not affected by the external restraints and thermal management techniques.

Introduction

Distortions induced by welding have been regarded as a critical issue in terms of performance, quality, and productivity. Many techniques have been developed to minimize the distortions induced by welding, such as external restraining, preheating, auxiliary side heating, heat sinking, and others. In general, most of the distortion mitigation techniques have been developed according to conventional understanding to explain their effectiveness in distortion controls, and then evaluated by comparing with test results. These con-

ventional understandings may include not only theoretical and mathematical knowledge, but also generally accepted knowledge from experience or analogy. For example, the concept of predeformation is based on direct intuition after observing the distortion patterns; welding-induced deformation is compensated for by the counterdeformation formed in joints prior to welding. The other example can be heat control techniques applying preheating or side heating in order to reduce the temperature gradient. Once the basic idea is tested and evaluated, a number of parametric studies may follow to find the optimum condition and explain the effect of mitigation parameters.

Masubuchi (Ref. 1) summarized methods for reducing distortions in welded joints based on the research. He reviewed the general distortion-reduction methods in terms of weld dimensions, joint designs, welding processes, multipass welding, constraints, welding sequences, intermittent welding, and peening. More detailed discussions on the effects of external restraints and thermal-pattern alterations were presented. Pavlovsky and Masubuchi (Ref. 2) reviewed the various distortion control methods studied by U.S.S.R. researchers. Conrardy and Dull (Ref. 3) reviewed the distortion control techniques applicable in thin ship panel structures. To reduce buckling, modifying panel design, applying intermittent welding, reducing heat input, and applying thermal tensioning were recommended. Restraining,

back-bending and backside line heating were recommended as techniques for reducing angular distortion.

Recently, the finite element method has been used to investigate the performance of various distortion control techniques, and has provided the fundamental understanding of the distortion mechanism and the effects of distortion control techniques on distortion patterns. Park (Ref. 4) developed a model to predict the thin plate panel distortion, and simulated the effect of welding sequences on the reduction of the distortions. Ohata et al. (Ref. 5) introduced the GTA preheating method to reduce the angular distortion in fillet welded aluminum thin plates, and performed weld tests and finite element analyses to evaluate its effectiveness. Michaleris and his coworkers (Refs. 6, 7) studied the effect of thermal tensioning buckling in panel structures using tests and finite element analysis. Ma et al. (Ref. 8) simulated the effects of weld sequences, a working table, and external restraints on the angular distortion of fillet welded T-joints, using 2-D finite element analysis. Han (Ref. 9) simulated the effects of side heating, heat sinking, and their combination on the distribution pattern of the longitudinal plastic strain associated with the longitudinal compressive stress causing buckling, using 2-D finite element analysis.

However, no rigorous studies have been carried out to investigate how these techniques affect the relationship between cumulative plastic strains and distortion. Recently, Han (Ref. 9) investigated how heat sinking and side heating affect the longitudinal cumulative plastic strain, and explained the effectiveness of the methods based on the relationship between the longitudinal cumulative plastic strain and the longitudinal residual stress associated with buckling in butt joint welded plates.

Jung (Ref. 10) developed the procedure, the so-called plasticity-based distortion analysis (PDA), which enables the investigation of the relationship between

KEYWORDS

Angular Distortion
Cumulative Plastic Strains
Gas Metal Arc Welding
Heat Sinking
Gas Tungsten Arc Preheating
T-Joints
Fillet Welds
Thermal Management Techniques

G. H. JUNG is with Edison Welding Institute, Columbus, Ohio. C. L. TSAI is with Industrial, Welding and Systems Engineering at The Ohio State University, Columbus, Ohio.

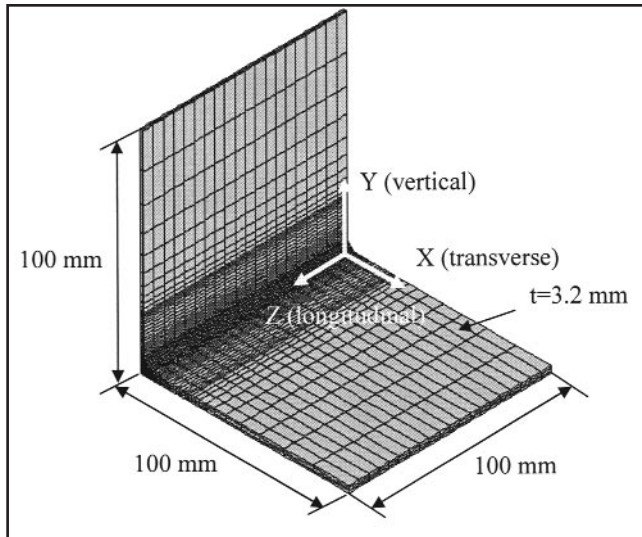


Fig. 1 — Symmetric half finite element model for the T-joint.

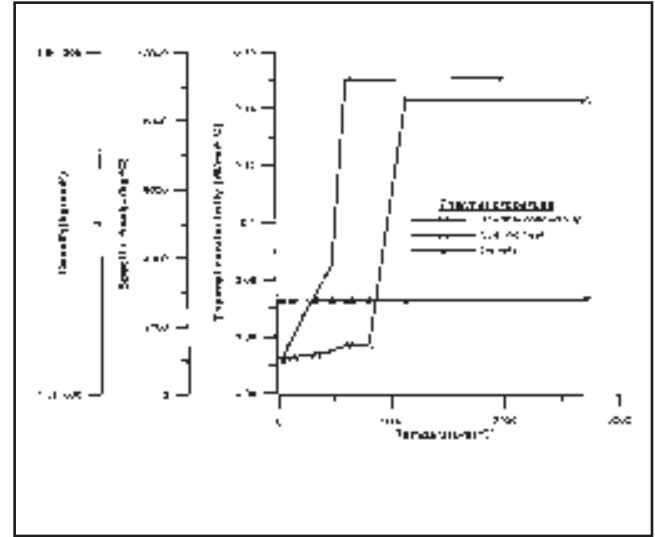


Fig. 2 — Temperature-dependent thermal material properties of magnesium Alloy AZ91 C.

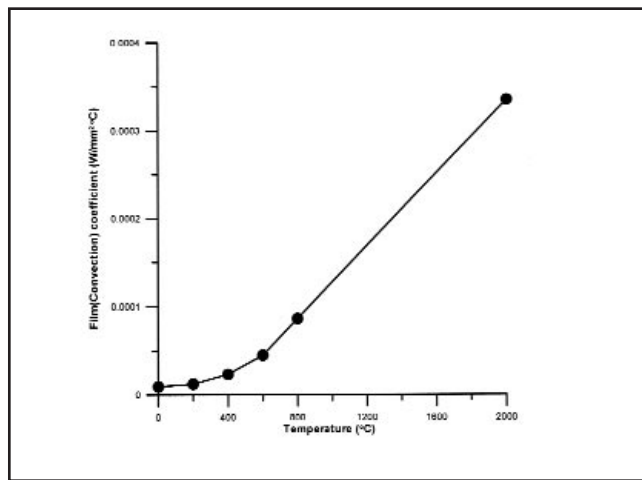


Fig. 3 — Temperature-dependent natural convection (film) coefficients.

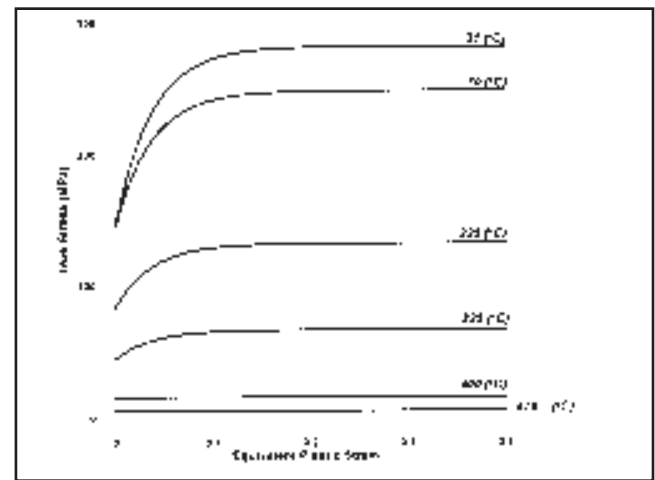


Fig. 4 — Temperature-dependent nonlinear kinematic strain-hardening model of magnesium alloy.

cumulative plastic strains and angular distortion in fillet welded T-joints. The PDA successfully explained each cumulative plastic strain's contribution to angular distortion in fillet welded T-joints.

This study investigated the effect of external restraints and two specific thermal management techniques (heat sinking and GTA preheating) on the relationship between cumulative plastic strains and angular distortion for fillet welded thin plate T-joints using PDA.

Plasticity-based Distortion Analysis (PDA) for Fillet Welded T-Joints

During welding, materials experience plastic deformation due to the thermal stresses induced by the temperature gradient, the external restraints, and the material softening. Plastic strains are cumulated during the plastic deformation, and then

remained permanently after temperature reaches room temperature and some temporary restraints are removed. These cumulative plastic strains result in residual stresses and distortions in the welded joints. The inherent shrinkage model is one of the methods to incorporate these cumulative plastic strains in the welded joints using the equivalent forces and moments, and to predict the welding-induced distortions without performing the thermal-elastic-plastic analysis (Refs. 11, 12). However, when the joint configuration is complex, such as T-joints, it is difficult to calculate the equivalent forces and moments because of the lack of knowledge about the relationship between cumulative plastic strains and distortions.

On the other hand, PDA enables us to predict distortions by mapping all cumulative plastic strains into elastic models using the equivalent thermal strains instead of the equivalent forces and mo-

ments, and provides the quantitative relationship between cumulative plastic strains and distortions.

The PDA includes the following three parts:

- Part 1: Thermal-elastic-plastic analyses (EPA) to obtain cumulative plastic components and distortions
- Part 2: Elastic analyses with thermal strains, which are equivalent to the cumulative plastic strains obtained from the EPA to predict the individual distortions that are associated with only one cumulative plastic strain component
- Part 3: Postprocessing to check the accuracy of the predicted distortion. If the accuracy does not satisfy the required accuracy, update a finite element model and repeat Parts 1, 2, and 3.

Thermal-Elastic-Plastic Analysis

The 3-D uncoupled thermal-elastic-

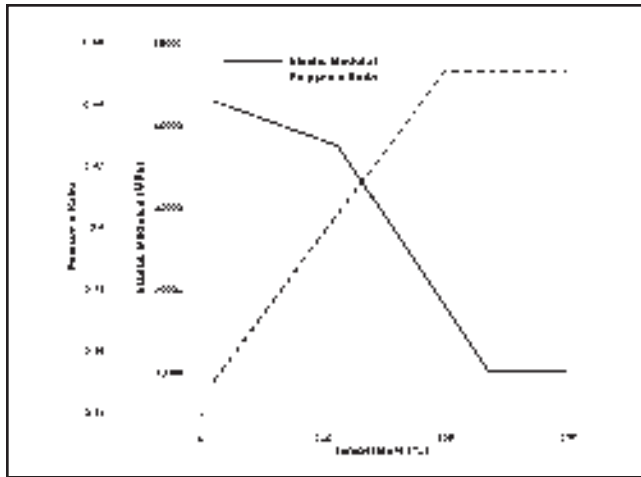


Fig. 5 — Temperature-dependent elastic modulus and Poisson's ratio of magnesium alloy.

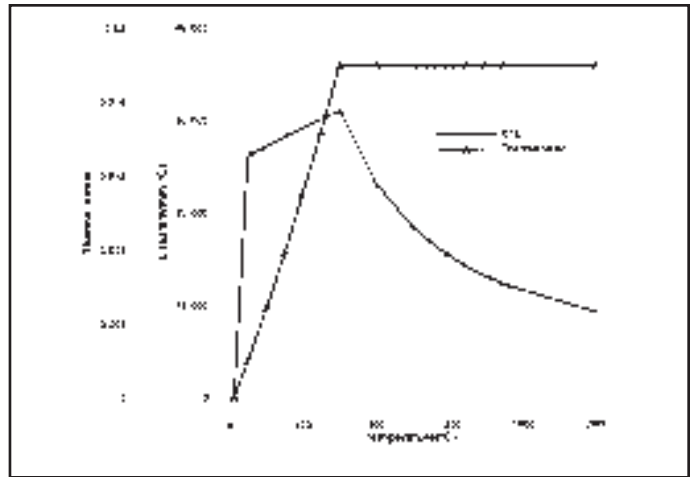


Fig. 6 — Temperature-dependent CTE and corresponding thermal strain of magnesium alloy.

plastic analysis for fillet welded T-joints without any external restraints and thermal management techniques was performed to obtain the baseline information, such as the characteristic distribution patterns of cumulative plastic strains and the corresponding angular distortion, using *ABAQUS* 5.8-14.

The material is magnesium Alloy AZ91 C, which application has been expanded because of its relatively lower density. In this study, weld tests were not performed; only numerical simulations were performed. It is assumed that the present analysis procedure provides the reasonable distribution patterns of the cumulative plastic strains and the corresponding angular distortion in fillet welded T-joints. The validity of the present EPA procedure was evaluated by comparing the angular distortions obtained from the EPA and experiments for aluminum fillet welded T-joints (Ref.10).

Two fillet welds running simultaneously at two sides constructed the T-joint. The given gas metal arc welding parameters were voltage = 13 V, current = 110 A, weld speed = 10 mm/s for 3.2-mm-thick plates (Ref. 13).

Figure 1 shows a symmetric half finite element model used in the EPA for a fillet welded T-joint, with a flange, 100 × 200 × 3.2 mm, and a web erected on the flange plate, 100 × 100 × 3.2 mm. Quadratic brick elements with 20 nodes, DC3D20 (thermal analysis), and C3D20R (elastic-plastic analysis) in *ABAQUS* (Ref. 14) were used. The total number of elements and nodes used were 6100 and 30,068, respectively.

Figure 2 shows the temperature-dependent thermal properties (Ref. 15). The latent heat, solidus, and liquidus temperature are 3.73E5 J/(kg°C), 470°C, and 595°C, respectively. Natural convection boundaries shown in Fig. 3 were described

Table 1 — Comparison of the Averaged Displacements Obtained from EPA, PDA, and Simultaneous Mapping Analysis for a T-Joint

Type of Analysis	Displacement (mm)			
	U_x	U_y	U_z	
EPA	-2.090E-01	1.042E+00	1.328E-01	
$\Sigma \epsilon^p_{xx}$	-1.694E-01	-1.143E+00	1.028E-01	
$\Sigma \epsilon^p_{yy}$	1.202E-02	-7.656E-01	5.590E-04	
$\Sigma \epsilon^p_{zz}$	-2.263E-04	8.392E-02	5.364E-03	
PDA	$\Sigma \epsilon^p_{xy}$	-4.991E-02	2.805E+00	1.088E-03
$\Sigma \epsilon^p_{sxz}$	-3.316E-04	9.435E-03	1.627E-01	
$\Sigma \epsilon^p_{yz}$	-4.742E-04	1.995E-02	-1.399E-01	
SUM	-2.084E-01	1.009E+00	1.327E-01	
Simultaneous Mapping	-2.084E-01	1.009E+00	1.327E-01	

on the entire free surfaces of the joint except for a symmetric plane. Figures 4–6 show mechanical properties depending on temperature. Nonlinear kinematic strain hardening proposed by Chaboche (Ref. 14, 17) was used.

The effect of a moving heat source was incorporated by the user-subroutine in *ABAQUS*, *DFLUX* (Ref. 14). Body flux had a double ellipsoidal distribution proposed by Goldak (Ref. 16). Heat input calibration was carried out by matching the boundary of the molten pool with the pre-designed fillet size. UVARM (Ref. 14) was developed to calculate the maximum peak temperature overall nodes. Figure 7 shows a map of the maximum peak temperature with a calibration factor of 0.6 including the arc efficiency. During the elastic-plastic analysis, symmetric boundary conditions were described on the YZ plane in Fig. 1, and the top free edge of the web plate was fixed. The effects of the filler metal deposition, the stress and strain relaxation at melting temperature, and metallurgical transformation were not considered in the present EPA.

The characteristic cumulative plastic strain distribution patterns and the associ-

ated angular distortion for fillet welded thin plate T-joints were obtained from the EPA. The angular distortion was defined by the displacement in the Y-direction (Fig. 1) at the free edge of the flange plate (at X=100 mm). The obtained averaged angular distortion from the EPA was 1.04 mm.

Elastic Analysis

The finite element model and mechanical boundary conditions used in the elastic analysis are the same as those of the EPA. The cumulative plastic strains obtained from the EPA were mapped into elastic models with the same nodes and elements, elastic modulus (4.3E4 [MPa]) and Poisson's ratio (0.35) at room temperature using the equivalent thermal strains.

Each cumulative plastic strain component can be mapped independently into six elastic models. Anisotropic thermal expansion coefficients and corresponding temperature fields replace the cumulative plastic strains. For example, the transverse cumulative plastic strain, $\Sigma \epsilon^p_{xx}(x,y,z)$ can be mapped by using the temperature field calculated by Equation 1 (Ref.14):

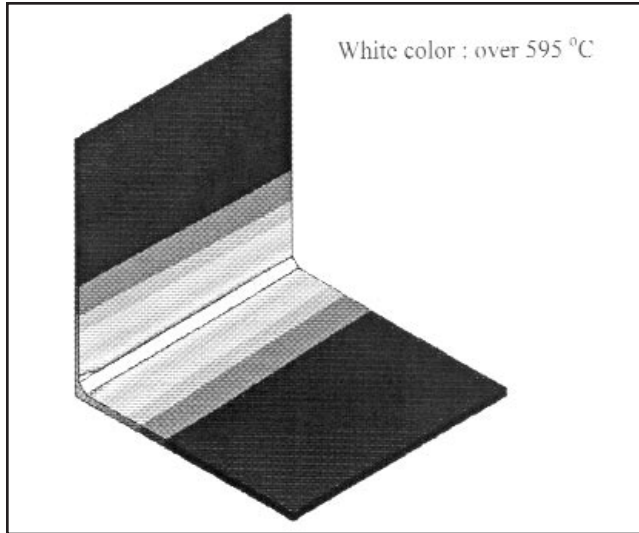


Fig. 7 — Maximum peak temperature map in the T-joint

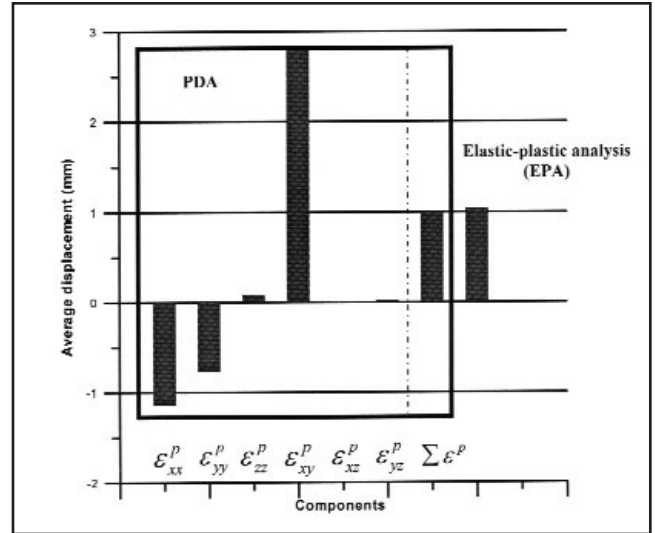


Fig. 8 — Averaged angular distortions calculated by EPA and PDA.

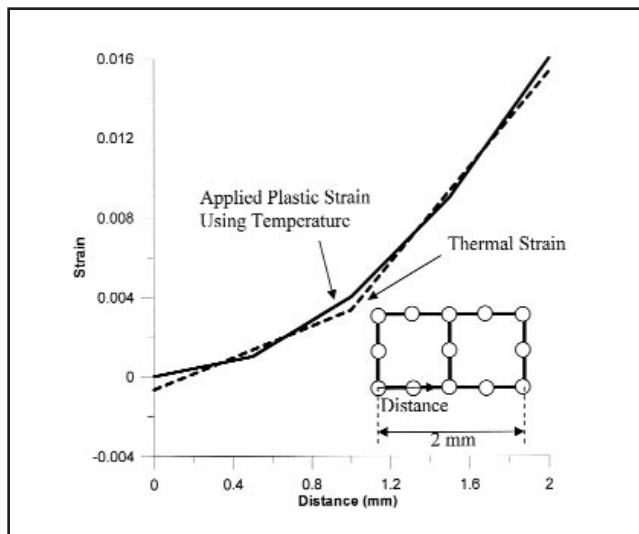


Fig. 9 — Characteristics of thermal strain in second-order elements

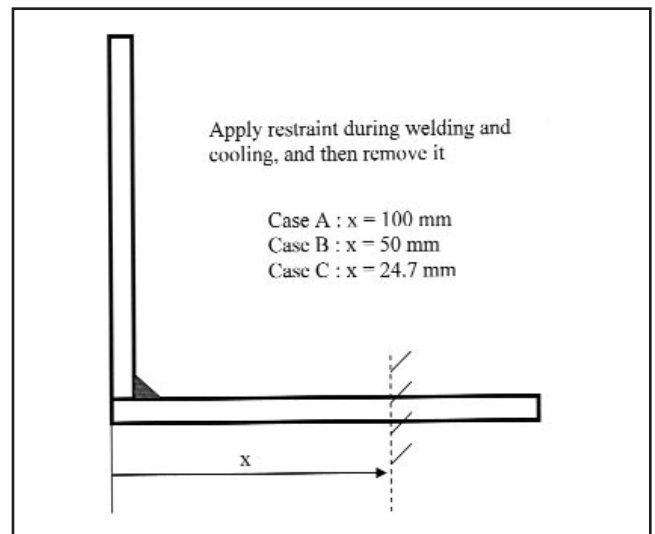


Fig. 10 — Locations of applied external restraints

$$\theta_{xx}(x, y, z) = \frac{\Sigma \epsilon_{xx}^p(x, y, z)}{\alpha_{xx}} \quad (1)$$

$$\alpha_{xx} = \text{constant}, \alpha_{yy} = \alpha_{zz} = \alpha_{xy} = \alpha_{xz} = \alpha_{yz} =$$

where $\Sigma \epsilon^p$ = averaged cumulative plastic strain at nodes, θ = temperature, a = anisotropic thermal expansion coefficients. Other temperature fields associated with other cumulative plastic strain components can be obtained using Equation 1 as well.

Six cumulative plastic strains can also be simultaneously mapped into an elastic model using the equivalent thermal strains depending upon six field variables defined by Equation 2 (Ref.14):

$$\epsilon_{ij}^{th} = \alpha_{ij} F_{ij}(x, y, z)$$

$$\text{where } F_{ij}(x, y, z) =$$

$$\frac{\Sigma \epsilon_{ij}^p(x, y, z)}{a_{ij}}; \text{ Field Variables} \quad (2)$$

This simultaneous mapping method was used to demonstrate the validity of the addition procedure to obtain the total distortion and the unique relationship between cumulative plastic strains and distortions.

Figure 8 also clearly shows the quantitative relationship between cumulative plastic strains and angular distortion. The transverse, $\Sigma \epsilon_{xx}^p$, and the vertical, $\Sigma \epsilon_{yy}^p$, cumulative plastic strain components result in the bend-down angular distortion, and the longitudinal, $\Sigma \epsilon_{zz}^p$, and the xy-plane

shear, $\Sigma \epsilon_{xy}^p$, cumulative plastic strain components generate the bend-up angular distortion. Most bend-up angular distortion is induced by the xy-plane shear cumulative plastic strain, and the angular distortion induced by other shear, $\Sigma \epsilon_{xz}^p$ and $\Sigma \epsilon_{yz}^p$, cumulative plastic strains is small enough to be negligible.

Postprocessing

The total distortion induced by all cumulative plastic strains is obtained by adding the individual distortions calculated from six independent elastic analyses:

$$\delta_{PDA}^{total} = \sum_{i=1}^6 \delta_i \quad (3)$$

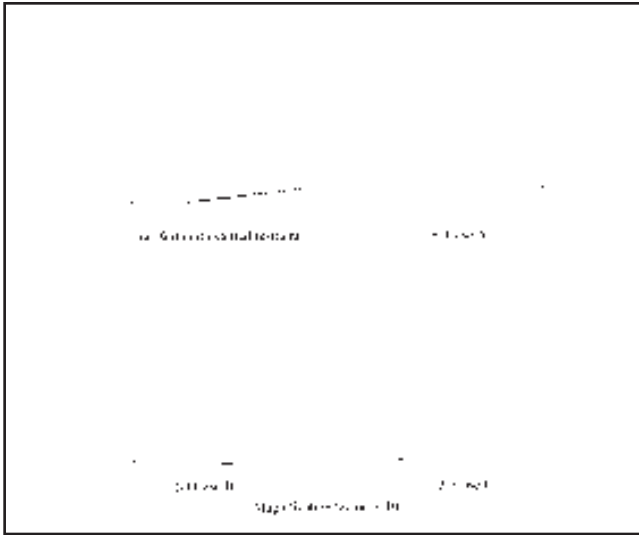


Fig. 11 — Deformed shapes after removing external restraints.

where δ_{total}^{PDA} = the total distortion, δ_i = the individual distortion with only i^{th} component of cumulative plastic strains. The accuracy of the PDA procedure can be determined by comparing the distortions from the EPA with the total distortions obtained from the PDA using Equation 3.

$$Error = \left| \frac{\delta_{EPA} - \delta_{PDA}^{total}}{\delta_{EPA}} \right| \times 100(\%) \quad (4)$$

This accuracy of the PDA procedure may be affected by some factors such as the nonlinearity of material and the mapping accuracy.

One factor is material nonlinearity, which does not allow the linear suppositions if the effect of nonlinearity is dominant. Material nonlinearity comes from the plastic deformation and the temperature dependency of material properties in the welding situation. In the PDA, material nonlinearity due to temperature dependency does not exist anymore because temperature is constant (room temperature) after completing welding. Nonlinearity due to the plastic deformation can also be negligible because the PDA is somewhat elastic, reloading analysis up to the final plastic deformation after welding.

The mapping accuracy may also affect the accuracy of the PDA procedure. The mapping accuracy is strongly dependent upon the number of elements/nodes and the order of shape function of element. Figure 9 shows the applied cumulative plastic strain using temperature and the calculated thermal strain within two second-order elements in which the thermal strain is linear. Unless the cumulative plastic strains are distributed uniformly or

linearly within an element, the mapping error is unavoidable even though second-order elements are used. The averaged cumulative plastic strains at nodes may also result in the error when significant discontinuity of the cumulative plastic strains at the integration points between the adjacent elements is present. In order to reduce the error induced by mapping, a finer-meshed model with second-order elements is recommended.

In this study, it was assumed that the acceptable error range of the PDA procedure was 0 to 10% in view of the engineering application. Since most error comes from the mapping, the finite element model should be updated until the required accuracy is achieved. The averaged total angular distortion obtained from the PDA was 1.01 mm, which had 3% error compared with 1.04 mm obtained from the EPA. This accuracy is acceptable.

In order to evaluate the PDA application to fillet welded T-joints and demonstrate the unique relationship between cumulative plastics and distortion, the simultaneous mapping analysis was performed under the combined cumulative plastic strains. Table 1 shows that the displacements obtained from the simultaneous mapping analysis are equal to those calculated by the PDA, which satisfies the linear superposition requirement described in Equation 5. Therefore, the PDA procedure is valid and each individual dis-

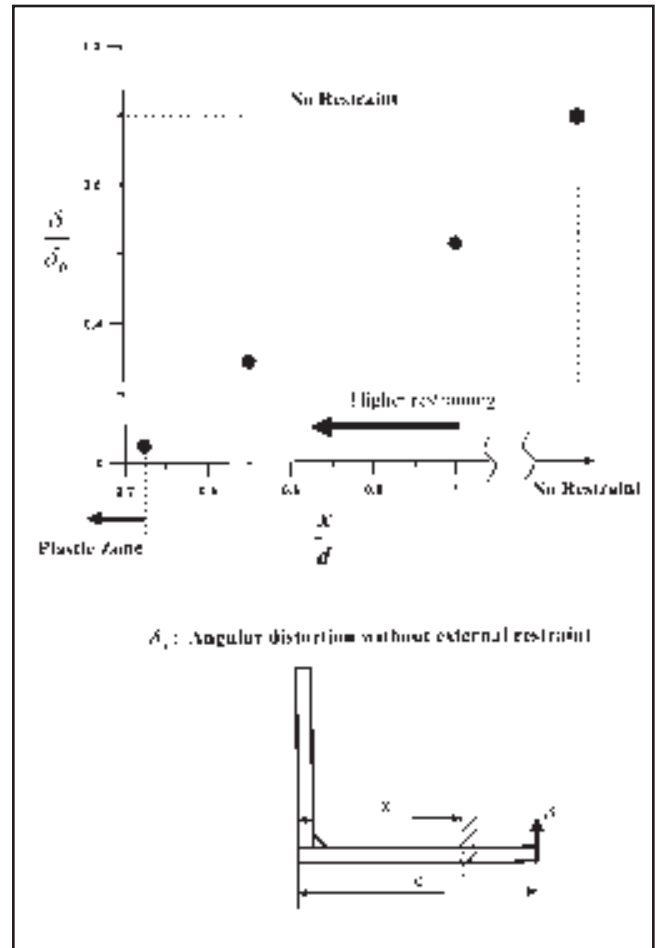


Fig. 12 — Comparison of averaged angular distortion for the cases with differing degrees of external restraint.

ortion can be uniquely determined by the associated cumulative plastic strain.

$$\begin{aligned} &L \left(\Sigma \epsilon_{xx}^p, \Sigma \epsilon_{yy}^p, \Sigma \epsilon_{zz}^p, \Sigma \epsilon_{xy}^p, \Sigma \epsilon_{xz}^p, \Sigma \epsilon_{yz}^p \right) \\ &= L_1 \left(\Sigma \epsilon_{xx}^p \right) + L_2 \left(\Sigma \epsilon_{yy}^p \right) + L_3 \left(\Sigma \epsilon_{zz}^p \right) \\ &+ L_4 \left(\Sigma \epsilon_{xy}^p \right) + L_5 \left(\Sigma \epsilon_{xz}^p \right) + L_6 \left(\Sigma \epsilon_{yz}^p \right) \quad (5) \end{aligned}$$

Effect of External Restraints on Angular Distortion in T-Joints

The external restraining techniques have been widely known as useful techniques for reducing the angular distortion in welded structures. For pressure vessels or large-scale pipes, pre-expanding has been adopted to reduce the radial shrinkage. In the case of T-joints, it has been reported that restraining and back-bending of the flange plates are effective means for reducing angular distortion (Ref. 3).

In this study, the PDA investigates the effect of external restraints on the characteristic relationship between cumulative

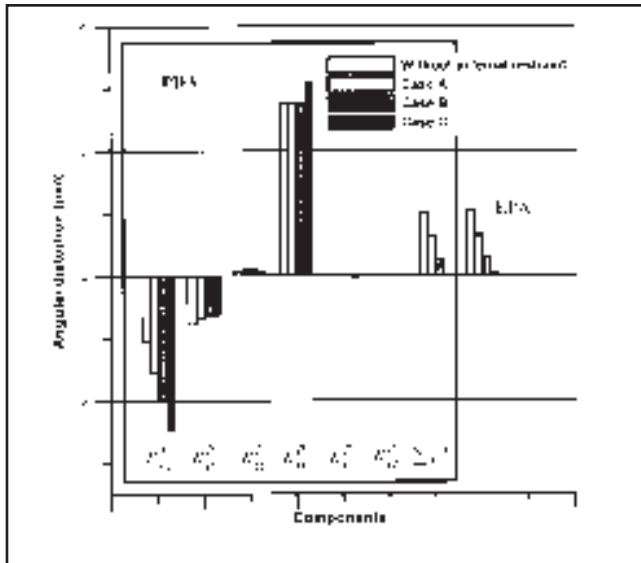


Fig. 13 — Comparison of averaged angular distortions calculated by EPA and PDA for the cases with differing degrees of external restraint.

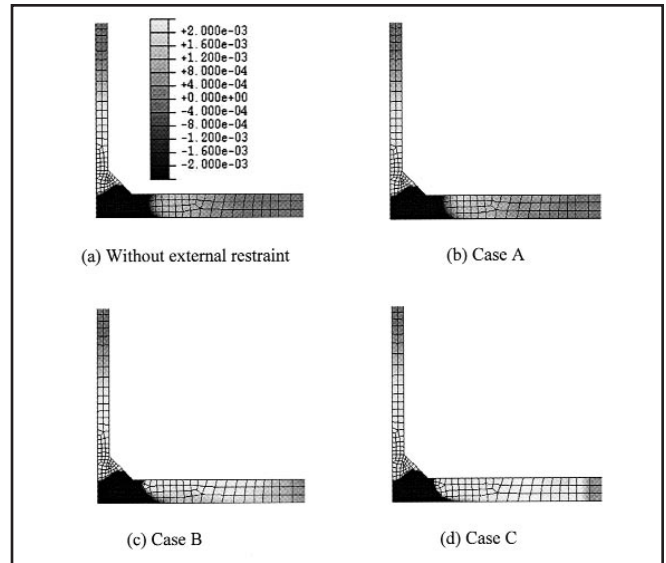


Fig. 14 — Transverse cumulative plastic strain maps for the cases with differing degrees of external restraint.

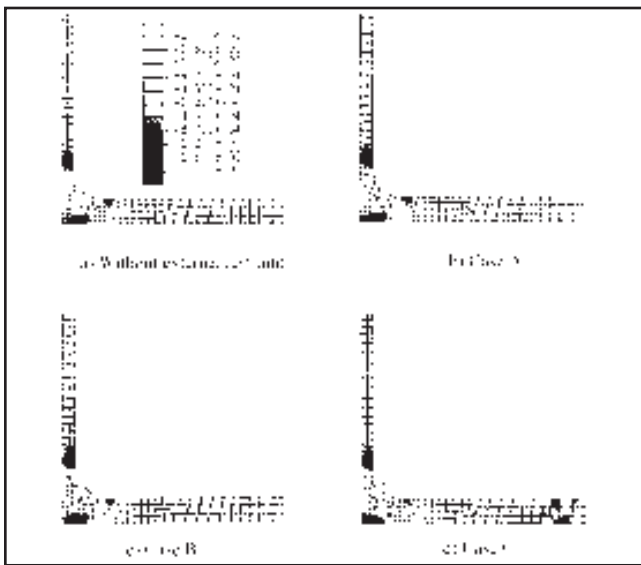


Fig. 15 — *xy*-plane shear cumulative plastic strain maps for the cases with differing degrees of external restraint.

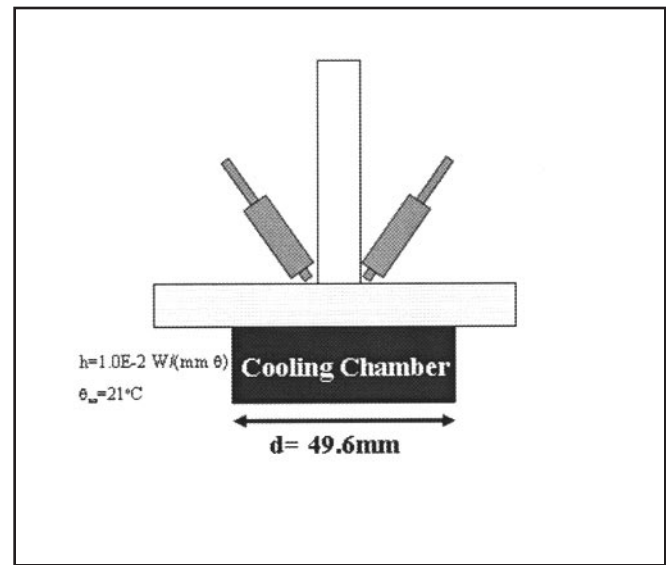


Fig. 16 — Scheme of heat sinking applied to the T-joint.

plastic strains and angular distortion in fillet welded T-joints.

Thermal Analysis (Part 1)

Some amount of heat loss through the contact surfaces between the fixtures and the flange may occur, but it was assumed that heat loss through the contact surfaces would be negligible. Therefore, the same temperature evolution obtained from the previous thermal analysis was used in the following elastic-plastic analyses for the three cases with differing degrees of external restraining.

Elastic-Plastic Analysis (Part 1)

It has been reported that the angular

distortion is affected by the degree of external restraining (Refs. 1, 18); the higher degree of restraining, the less angular distortion. In this study, external restraints were applied along the flange plate with fixed boundary conditions. The degree of restraining is inversely proportional to the distance between the weld interface and the line of the fixed boundaries.

Figure 10 shows the locations of external restraints. Three cases designated as Case A, Case B, and Case C have differing degrees of external restraining. The locations applying the fixed boundary conditions for Case A, Case B, and Case C were $x = 100$ mm, 50 mm, and 24.7 mm, respectively. Case C has the highest restraining of the three cases. These fixed boundary conditions were applied during

heating and cooling, and then removed after cooling was completed. The final angular distortion was obtained after removing external restraints. From these simulations, we can obtain the characteristic cumulative plastic strain distribution patterns and the angular distortion associated with differing degrees of external restraining, both of which can be used in the PDA to investigate the effect of the external restraints on the angular distortion in T-joints.

Figure 11 shows the deformed shapes after removing the external restraints with the same scaling factor. The averaged angular distortions for Cases A, B, and C are 0.65, 0.30, and 0.05 mm, respectively. They are plotted in Fig. 12 with dimensionless parameters. Figures 11 and 12 show that

less angular distortion is expected at a higher degree of restraining. A minute angular distortion is produced in Case C with external restraints at $x = 24.7$ mm where it is close to the boundary of the plastic zone ($x = 21.58$ mm) produced in the case without external restraints.

These differences among the three cases may result from the change in the cumulative plastic strain distributions due to the external restraints. The effects of the external restraints on the distribution patterns of the cumulative plastic strains can be observed by plotting the cumulative plastic strains. However, this observation may not give the right and quantitative interpretation of the relationship because the cumulative plastic strains have complicated distribution on the welded region. Therefore, the PDA was carried out to study the effect of the external restraints on the characteristic relationship between cumulative plastic strains and angular distortion.

Elastic Analysis and Postprocessing (Parts 2, 3)

The cumulative plastic strains obtained from the three cases with differing degrees of external restraining were mapped into elastic models using the equivalent thermal strains.

In order to investigate the effect of external restraints on the relationship between cumulative plastic strains and angular distortion, the individual and the total angular distortions for the three cases and a case without external restraints are plotted together in Fig. 13. Reasonable accuracy of the PDA is shown for all cases.

No change of the basic relationship between cumulative plastic strains and angular distortion is observed: bend-down angular distortion is due to transverse/vertical cumulative plastic strains, bend-up angular distortion is due to longitudinal/xy-plane shear cumulative plastic strains, and no angular distortion is caused by other shear cumulative plastic strains.

The major change due to the external restraints is observed in the individual angular distortion induced by the transverse cumulative plastic, $\Sigma \epsilon_{xx}^p$. A higher degree of restraining produces a more bend-down angular distortion induced by the transverse cumulative plastic strain. Figure 14 shows the change in the transverse cumulative plastic strain distributed on the flange plate. There is no change in the distribution on the web plate, but the area with the positive plastic strain on the top surface of the flange expands with an increase in the degree of restraining. The positive transverse plastic strain presents within the plastic zone where the compressive longitudinal plastic strain exists.

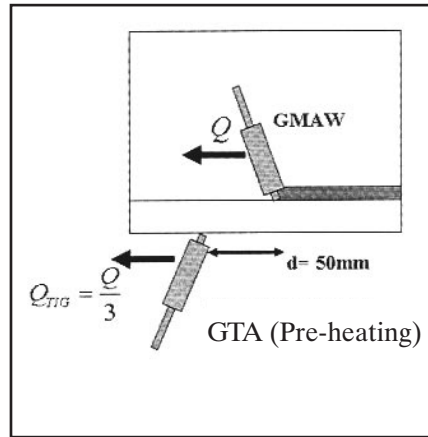


Fig. 17 — Scheme of GTA preheating applied to the T-joint.

Some parts of the positive transverse plastic strain may originate to satisfy the incompressibility under the plastic deformation. However, the applied external restraints (transverse and bending restraining) may not significantly affect the distribution of the longitudinal cumulative plastic strain because the longitudinal stress is mostly governed by the longitudinal restraint or the rigidity in the longitudinal direction. Therefore, considering the distribution pattern of the positive transverse plastic strain, yielding may occur due to the high tensile transverse stress, which is generated by the external restraints that are present from the bend-up bending and the transverse shrinkage during cooling. In general, higher restraining produces more cumulative plastic strains because higher stress resulting from higher restraining causes an earlier yielding. As higher external restraining is applied, higher and wider positive transverse cumulative plastic strain is produced and more bend-down angular distortion occurs because the role of the positive transverse cumulative plastic strain on the top surface of the flange bends down the flange plate.

For the vertical cumulative plastic strains, $\Sigma \epsilon_{yy}^p$, only a slight change in the angular distortion is shown. In general, less bend-down angular distortion is induced by higher external restraining. No change in the angular distortion induced by the longitudinal cumulative plastic strain occurs. This may imply that the external restraints applied on the flange would not affect the distribution patterns of the longitudinal cumulative plastic strain.

For the angular distortion induced by the xy-plane shear cumulative plastic strain, $\Sigma \epsilon_{xy}^p$, no change in the individual angular distortion is shown except Case C with the external restraint close to the

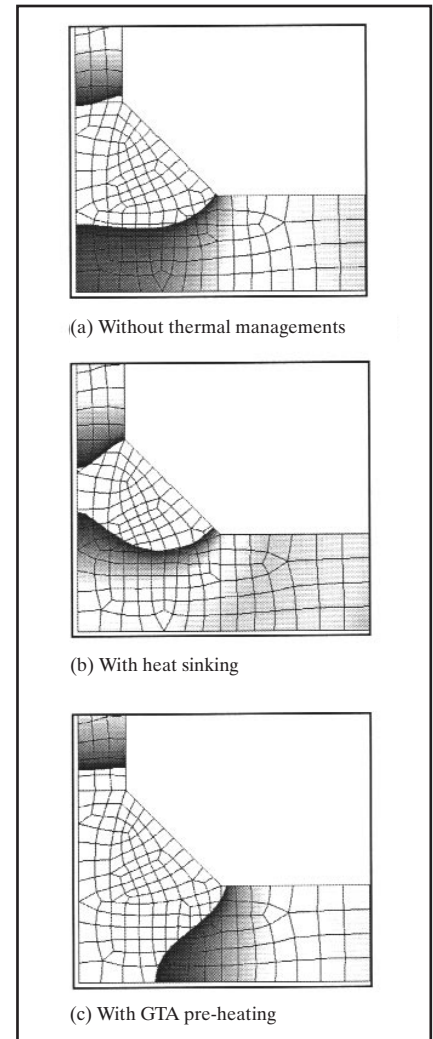


Fig. 18 — Comparison of nugget shapes obtained from thermal analyses with different thermal management techniques.

boundary of the plastic zone. Figure 15 clearly shows how the external restraints affect the distribution of the xy-plane shear cumulative plastic strain. There is no change in the distribution pattern for Case A, Case B, and the case without external restraints. For Case C, the external restraint close to the boundary of the plastic zone disturbs the distribution of the xy-plane shear cumulative plastic strain. The change in the individual angular distortions induced by other shear components is negligible.

Based on results of the PDA, it can be concluded that the reduction of the angular distortion by the external restraints applied on the flange results from an increase of the bend-down angular distortion induced by the transverse cumulative plastic strain. The region where the positive transverse cumulative plastic strain exists is expanded by increasing the degree of external restraining.

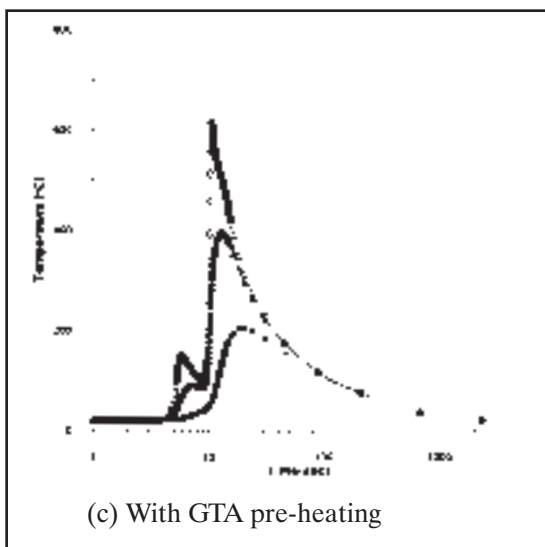
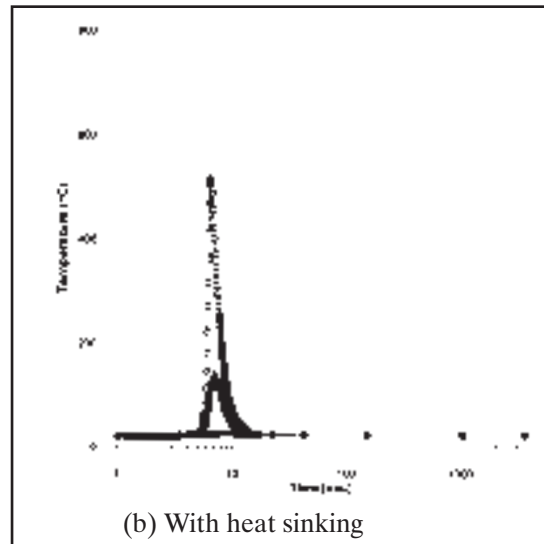
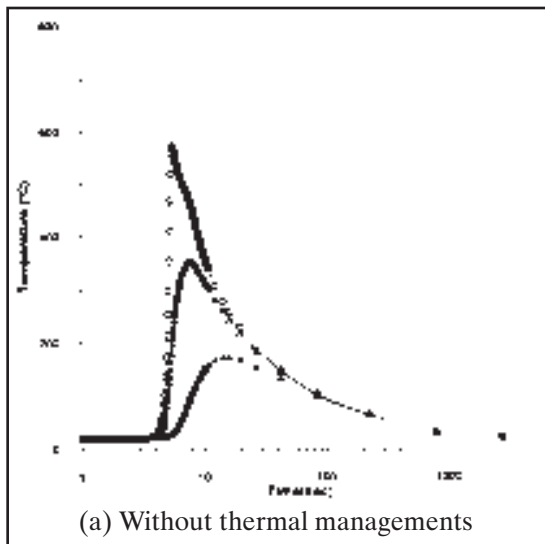


Fig. 19 — Comparison of temperature evolutions for the cases with different thermal management techniques.

Effect of Thermal Management Techniques on Angular Distortion in T-Joints

Two thermal management techniques were selected: heat sinking and GTA preheating. They are inherently different in terms of heat control. Heat sinking reduces the heat-affected zone by applying a cooling chamber beneath the bottom of the flange. On the other hand, GTA preheating increases the heat-affected zone by preheating, which is carried out by running a gas tungsten arc ahead of gas metal arc welding (GMAW) on the bottom surface of the flange.

It has been reported that heat sinking is an effective way to reduce buckling (Ref. 7), and GTA preheating reduces the angular distortion in T-joints (Ref. 5). Most research has been focused on showing their effectiveness using weld tests

and numerical simulations. Recently, Han (Ref. 9) investigated the relationship between cumulative plastic strains and buckling for butt joints. However, it is still unknown how thermal management techniques affect the relationship between cumulative plastic strains and angular distortion in T-joints. Therefore, the effect of thermal management techniques on the relationship between cumulative plastic strains and angular distortion was investigated using the PDA.

Thermal Analysis (Part 1)

The effect of heat sinking was simulated by applying the relatively low film coefficient, $1.0E-2 \text{ W}/(\text{mm}^2 \text{ } ^\circ\text{C})$ with temperature 21°C , on the bottom surface of the flange within $x = 0\text{--}24.8 \text{ mm}$ as shown in Fig. 16. Gas tungsten arc preheating was modeled by running a gas tungsten arc 50 mm ahead of GMAW at the same speed as GMAW on the bottom surface of the flange as shown in Fig. 17. The GTA heat was one-third of that of GMAW, $477 \text{ W} (= 110 \text{ V} \times 13 \text{ A} \times \frac{1}{3})$ with a heat input calibration factor of 0.6.

A nugget with heat sinking will be smaller than that with GTA preheating because preheating raises the temperature in and around the weld region. Figure 18 shows the maximum peak temperature maps calculated by the user-subroutine, UVARM. Compared to the nugget without thermal management, heat sinking generates a smaller nugget and GTA preheating gives a larger nugget.

Heat management techniques affect not only the size of the heat-affected zone, but also the rate of heating and cooling, which can be related to the instantaneous

gradient of temperature in the plates. In general, heat sinking results in a higher temperature gradient due to a higher cooling rate, and facilitates achieving a uniform temperature in the plates compared to the case without thermal management. Contrarily, GTA preheating increases the maximum peak temperature and reduces the temperature gradient.

Figure 19 compares temperature evolutions on three points located on the top surface of the flange, $x = 4.8, 9.8,$ and 24.8 mm . The distance between the curves represents the temperature gradient and their slopes show the heating and cooling rate. For heat sinking, a significant change of the magnitude of the maximum peak temperature, the temperature gradient, and the rate of cooling are observed. Gas tungsten arc preheating does not give significant changes in the temperature gradient and the cooling rate compared with the case without thermal management. During heating, two spikes on each curve show the effect of GTA preheating. Preheating also increases the maximum peak temperatures of each curve, which results in a wider nugget and heat-affected zone.

Based on the results of the thermal analysis, the two thermal management techniques, heat sinking and GTA preheating, may give the opposite impact on not only the temperature evolution and profile, but also the angular distortion.

Elastic-Plastic Analysis (Part 1)

All boundary conditions for the two cases were the same as those of the case without the external restraints described in the previous section. The temperature evolutions for the two cases calculated by the thermal analyses were retrieved and applied to the elastic-plastic analysis.

Figure 20 shows the deformed shapes for the three cases with the same magnification scale factor: Case 1 = without ther-

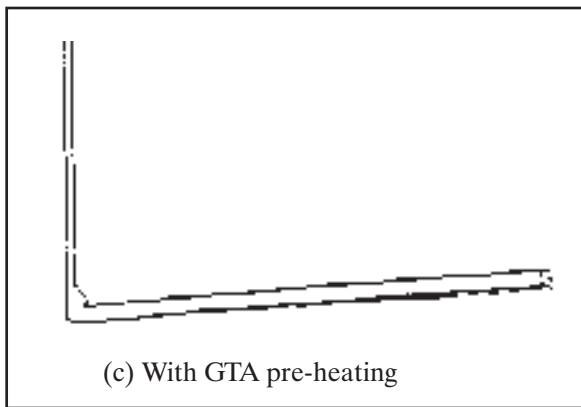
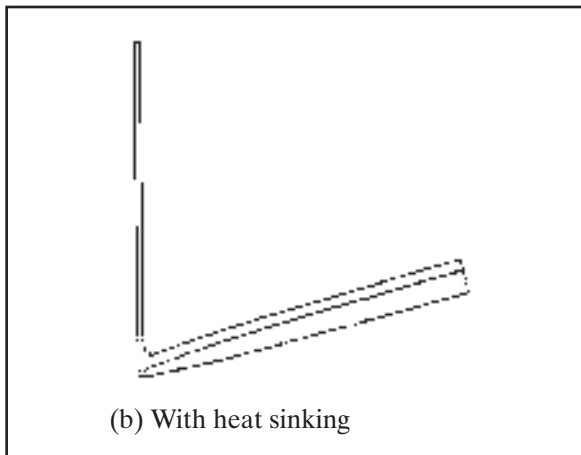
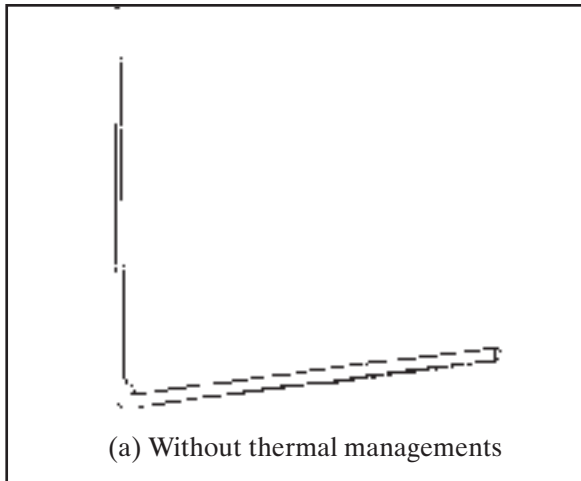


Fig. 20 — Comparison of deformed shapes for the cases with different thermal management techniques.

mal management, Case 2 = heat sinking, Case 3 = GTA preheating. The average angular distortions calculated for Cases 1, 2, and 3 are 1.04, 2.75, and 0.5 mm, respectively, and are plotted with dimensionless parameters in Fig. 21. It shows that heat sinking increases angular distortion, but GTA preheating reduces angular distortion. This opposite effect between the two thermal management techniques on the angular distortion was expected after observing the results of the thermal analysis. Figure 21 shows that external re-

straining and GTA preheating effectively reduces the angular distortion. The effect of the combination of GTA preheating and external restraining (Case A, restrained at $X = 100$ mm) was also tested, but a slight increase in the angular distortion was obtained compared to the case with only GTA preheating.

To investigate the causes of these differences, cumulative plastic strain maps for the three cases are plotted in Fig. 22. For Cases 1 and 3, a similar distribution pattern of the cumulative plastic strain is shown. On the other hand, a significant reduction of the size of the plastic zone is obtained by heat sinking. The distribution pattern of the transverse cumulative plastic strain for Case 2 is different from those of Cases 1 and 3. For Case 2, the transverse cumulative plastic strain on the top surface of the flange is wider than on the bottom of the flange, which may cause the bend-up angular distortion and eventually reduce the amount of the bend-down angular distortion. For the vertical cumulative plastic

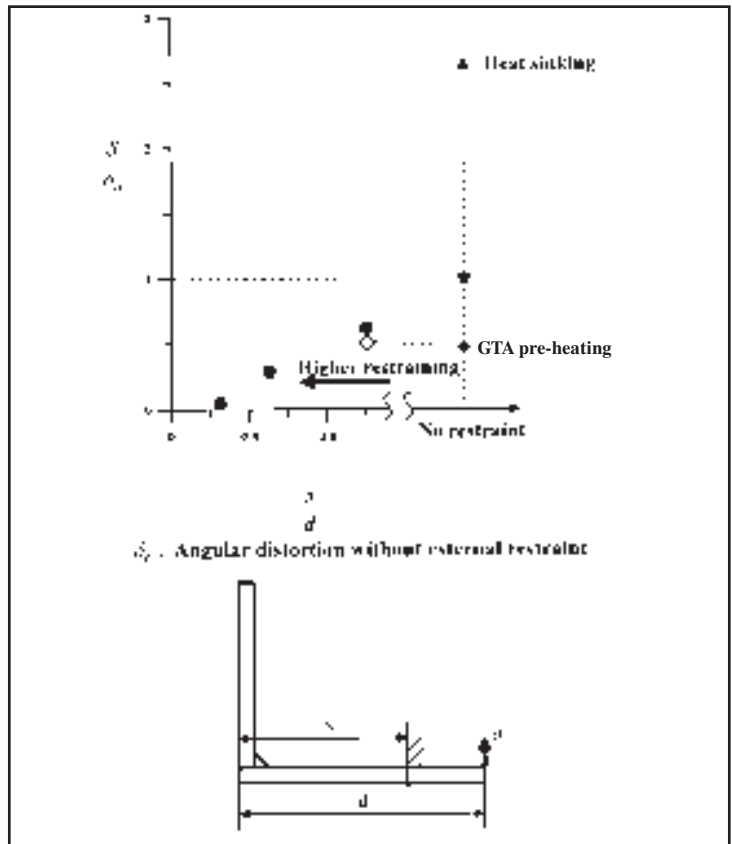


Fig. 21 — Comparison of averaged angular distortions for the cases with different distortion control plans.

straining, the reduced size of the plastic strain zone in the flange may affect the angular distortion as well. Even though there is significant change in the distribution pattern of the longitudinal cumulative plastic strain, the resultant effect may be small because the longitudinal component is not as sensitive as other components on the angular distortion. For the xy-plane shear cumulative plastic strain, no significant change is shown. For Case 3, it is not clear what causes the reduction of the angular distortion because there is no significant difference of cumulative plastic strain distributions between Cases 1 and 3. Compared to other components, it is observed that the distribution of the xy-plane shear cumulative plastic strain is slightly affected by GTA preheating. Gas tungsten arc preheating increases the area of the positive shear strain region on the bottom (or corner) of the flange and the area of the negative shear strain region on the top of the flange. However, it is not clear if this observation and interpretation is right at this point.

Elastic Analysis and Postprocessing (Parts 2 and 3)

As discussed previously, it is not easy to figure out the relationship between cumu-

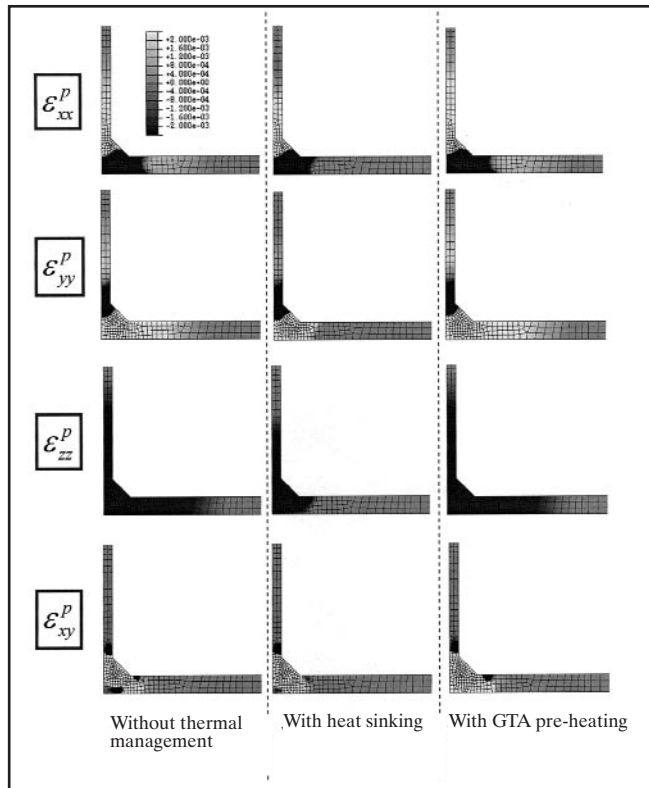


Fig. 22 — Comparison of typical cumulative plastic strain distribution patterns in the cases with different thermal management techniques.

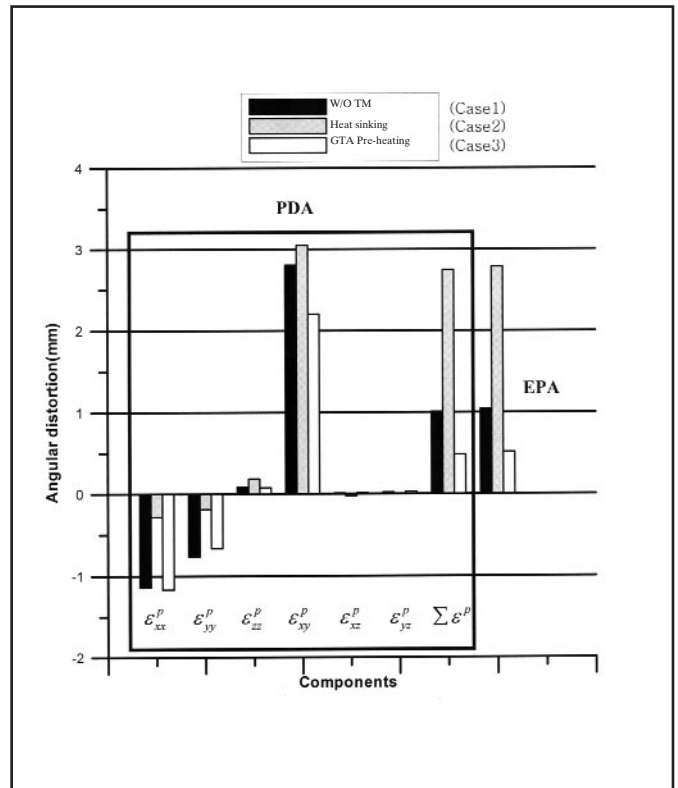


Fig. 23 — Comparison of averaged angular distortions calculated by EPA and PDA for the cases with different thermal management techniques.

lative plastic strains and angular distortion using only the results from the EPA. The PDA was performed to investigate the effect of the thermal management techniques on the relationship between cumulative plastic strains and angular distortion.

The individual and the total angular distortions are plotted and compared for Cases 1, 2, and 3 in Fig. 23. No matter what types of thermal management techniques are applied, the basic characteristic relationship between cumulative plastic strains and angular distortion is not changed: transverse and vertical cumulative plastic strains result in bend-down angular distortion, and longitudinal and xy-plane shear cumulative plastic strains generate bend-up angular distortion.

Figure 23 shows that heat sinking increases the bend-up individual angular distortion, reducing the bend-down angular distortion, and ultimately causing an increase in the total angular distortion. The main cause of the increase of the total angular distortion comes from the reduction of the bend-down angular distortion induced by the transverse and the vertical components. A relatively small increase of the angular distortion due to the longitudinal and the xy-plane shear components is shown. These results obtained from the PDA are similar to the ones discussed in the EPA based on the maps of the cumu-

lative plastic strains, but provide more quantitative information.

On the other hand, GTA preheating does not significantly change the individual angular distortions except the one induced by the xy-plane shear cumulative plastic strain. The reduction of the total angular distortion by GTA preheating is mainly related to the reduced bend-up angular distortion induced by the xy-plane shear cumulative plastic strain only. In order to reduce the bend-up angular distortion, the negative xy-plane shear strain resulting in the bend-down angular distortion must act more dominantly to reduce the bend-up angular distortion than the positive one. Therefore, the wider region of the negative xy-plane shear cumulative plastic strain on the top surface of the flange as shown in Fig. 22, the smaller bend-up angular distortion.

Based on results from the PDA, it can be concluded that heat sinking increases the total bend-up angular distortion by reducing the bend-down angular distortions induced by the transverse and the vertical cumulative plastic strains, and GTA preheating reduces the total bend-up angular distortion by reducing the bend-up angular distortion induced by the xy-plane shear cumulative plastic strain.

In addition, in terms of optimizing the welding-induced distortion, the selection of thermal management techniques

should be carefully performed. Based on this study, heat sinking can help to reduce buckling, but may result in more angular distortion. On the other hand, GTA preheating can reduce the angular distortion, but it may possibly result in buckling or a more transverse shrinkage because GTA preheating generates a wider plastic zone (Ref. 9).

Conclusions

The effect of external restraints and thermal management techniques on the relationship between cumulative plastic strains and angular distortion in fillet welded thin plate T-joints was discussed using results from the PDA. The major findings are summarized as follows.

1) The PDA successfully investigated the effect of the external restraints and the thermal management techniques on the relationship between cumulative plastic strains and angular distortion.

2) Angular distortion was reduced by increasing the degree of external restraining applied on the flange of T-joints. The PDA showed that the reduction of the angular distortion by external restraints resulted from the increase of the bend-down angular distortion induced by the transverse cumulative plastic strain. The effect of the external restraints on other cumulative plastic strains was small enough to

be negligible.

3) Heat sinking increased the angular distortion. The PDA showed that heat sinking mainly controlled nominal cumulative plastic strains, such as transverse, vertical, and longitudinal components. The bend-down angular distortion induced by the transverse and the vertical components was reduced by heat sinking, which resulted in the increase in angular distortion. For other components, the change in angular distortion was relatively small, thus negligible.

4) Preheating with a gas tungsten arc reduced the angular distortion. The PDA showed that GTA preheating mainly controlled the contribution of the xy-plane shear cumulative plastic strain existing in and around the welded region. The reduction in angular distortion resulted from the reduction of the bend-up angular distortion induced by the xy-plane shear cumulative plastic strain.

References

1. Masubuchi, K. 1980. *Analysis of Welded Structures*. Pergamon Press.
2. Papazoglou, V. J., and Masubuchi, K. 1982. Numerical analysis of thermal stresses during welding including phase transformation effects. *Transactions of the ASME, Journal of Pressure Vessel Technology*, 104: 198–203.
3. Conrardy, C., and Dull, R. 1997. Control of distortion in thin ship panels. *Journal of Ship Production* 13(2): 85–92.
4. Park, S. C. 1998. Distortion mechanisms and control methodology for welding thin-plate panel structures. Ph.D. thesis, The Ohio State University, Columbus, Ohio.
5. Ohata, M., Toda, Y., Toyoda, M., and Takeno, S. 1999. Control of welding distortion in fillet welds of aluminum alloy thin plates. *Welding International* 13(12): 967–976.
6. Michaleris, P., and Debicari, A. 1997. Prediction of welding distortion. *Welding Journal* 76(4): 172-s to 181-s.
7. Michaleris, P., and Sun, X. 1997. Finite element analysis of thermal tension techniques mitigating weld buckling distortion. *Welding Journal* 76(11): 451-s to 457-s.
8. Ma, N. X., Ueda, Y., Murakawa, H., and Maeda, H. 1995. FEM analysis of 3-D welding residual stresses and angular distortion in T-type fillet welds. *Transactions of JWRI* 24(2): 115–122.
9. Han, M. S. 2002. Fundamental studies on welding-induced distortion in thin plate. Ph.D. dissertation, The Ohio State University, Columbus, Ohio.
10. Jung, G. H. 2003. Plasticity-based distortion analysis for fillet welded thin plate T-joints. Ph.D. dissertation, The Ohio State University, Columbus, Ohio.
11. Ueda, Y., and Yuan, M. G. 1993. Prediction of residual stresses in butt welded plates using inherent strains. *Transactions of the ASME, Journal of Engineering Materials and Technology* 115(10): 417–423.
12. Yuan, M. G., and Ueda, Y. 1996. Prediction of residual stresses in welded T- and I-joints using inherent strains. *Journal of Engineering Materials and Technology* 118(4): 229–234.
13. *ASM Handbook* Volume 6. 2000. Welding, Brazing, and Soldering. ASM International.
14. *ABAQUS User's Manual*. 1998. HKS Co., USA.
15. Mg Database. International Magnesium Association. (<http://www.intlmag.org/>)
16. Goldak, J., Charkravarti, A., and Bibby, M. 1984. New finite element model for welding heat sources. *Metallurgical Transactions B* 15B: 300–305.
17. Chaboche, J. L. 1986. Time independent constitutive theories for cyclic plasticity. *International Journal of Plasticity* 2(2): 247–302.
18. Sizemore, J. 1994. Control of residual stresses and distortion in thin section panel fabrication: Review of welding processes and procedures Revision A. Ingalls Shipbuilding.

CALL FOR PAPERS WELDING FOR PIPELINE AND ENERGY APPLICATIONS SYMPOSIUM

Papers are sought on the welding and joining of products and components related to pipeline and energy applications. Authors are encouraged to submit a 500 to 1,000-word abstract by July 30th, 2004, to be considered for presentation at the 2005 Symposium on Welding for Pipeline and Energy Applications. The two-day Symposium is taking place in conjunction with the 53rd annual AWS Welding Show, April 26 through April 28 at the Dallas Convention Center in Dallas, Texas.

Papers representing original experimental investigations, theoretical and statistical modeling, and applications in welding and joining for pipeline and energy applications are sought in the following areas:

- Properties and structural integrity of weldments
- Design and manufacture of welded structures
- Corrosion of weldments
- NDE of weldments
- Weldability of high-strength steel and aluminum alloy pipelines
- Weld phase transformations & microstructures
- Dissimilar welding and joining of graded materials
- Welding processes and procedures
- Innovative welding consumables
- Sensing, control and automation
- Computer modeling and simulation
- Advanced and alternative joining technologies
- Robotics and automation
- Application studies
- Others

To submit your abstract for consideration or for more information on the Symposium on Welding for Pipeline and Energy Applications, and all AWS programs and conferences, visit www.aws.org/conferences or contact Dorcas Troche, manager, conferences and seminars, via e-mail at dorcas@aws.org, or 800-443-9353, ext.313.